

Cite this: *J. Mater. Chem. A*, 2016, 4, 14298

Integrated self-charging power unit with flexible supercapacitor and triboelectric nanogenerator†

Yu Song,^a Xiaoliang Cheng,^a Haotian Chen,^{ab} Jiahuan Huang,^a Xuexian Chen,^{ab} Mengdi Han,^a Zongming Su,^a Bo Meng,^a Zijian Song^a and Haixia Zhang^{*ab}

With the rapid development of wearable devices and portable electronics, highly efficient and stable self-powered systems are in great demand. However, most harvesting and storage devices of such systems are separate units, which reduce the power density and limit their applications. In this work, we implemented an integrated sandwich-shaped, self-charging power unit (SCPU) with a wrinkled PDMS-based triboelectric nanogenerator and CNT/paper-based solid-state supercapacitor. During ambient vibration process, this SCPU could simultaneously harvest and store energy, efficiently converting mechanical energy into electrochemical energy. The self-charging capability of this SCPU is demonstrated by periodic compressive stress, charging 900 mV within 3 h. Additionally, using three serially connected SCPUs as power supply, it could drive a commercial calculator working continuously and an electrochromic device as a smart window during the coloration and bleaching processes. Considering its efficient structure and facile fabrication, this novel integrated SCPU provides a feasible solution for sustainable power supply and shows great potential in micro-energy fields and self-powered systems.

Received 11th July 2016
Accepted 19th August 2016

DOI: 10.1039/c6ta05816g

www.rsc.org/MaterialsA

Introduction

As is well-known, energy crises are becoming a worldwide problem, and researchers are conducting every effort to exploit sustainable and renewable energy.¹ Environmental green energy sources exist in various forms, such as thermal,² biochemical,³ and solar.⁴ However, traditional energy systems require complicated external circuits and power management, which bring difficulties to miniaturized device applications. Besides the above energy forms, mechanical energy may be the most widely distributed energy form, existing all over our living environment.⁵ The micro-energy system based on mechanical energy conversion can sufficiently satisfy the needs of small-sized, portable electronics.^{6,7}

Energy harvesting⁸ and storage,⁹ as the two most crucial technologies for energy systems, are usually two different and independent devices based on two consecutive processes. Among different conversion methods of mechanical energy harvesting, the existing transduction mechanisms include piezoelectricity,^{10,11} electromagnetic induction,^{12,13} and electrostatic induction.^{14,15} Recently, a novel energy-harvesting device termed the triboelectric nanogenerator (TENG) has been

developed,^{16–19} the working mechanism of which is based on the coupling effect of contact electrification and electrostatic induction. It can efficiently scavenge mechanical energy from human motion or ambient vibrations with the advantages of high output, simple design, and low cost. Among various paths to enhance the performance of TENGs, both the modification of surface material²⁰ and introduction of micro/nanostructure²¹ play significant roles. To combine these two methods to further increase the surface charge density, wrinkle structures formed on the polymer are becoming increasingly important, with their simple fabrication, flexibility and adaptation for large-area patterns.^{22,23} Additionally, as for energy storage devices, the supercapacitor (SC) has been considered as one of the most promising candidates, attributed to its high power density, long cycle lifetime, and safety.^{24,25} In order to meet the great demand for portable/wearable personal electronics and flexible devices, the solid-state supercapacitor (SC)^{26,27} has been established by sandwiching a solid-state gel electrolyte between positive and negative electrodes on flexible substrates, such as paper²⁸ and carbon foam.²⁹ Compared to the conventional SCs with liquid electrolytes,³⁰ the solid-state SCs avoid the possibility of electrolyte leakage and short circuit of the two electrodes.

To combine energy harvesting and storage, different types of self-powered systems^{31–33} have been proposed by collecting energy from the ambient environment to continuously supply sensors. However, most harvesting and storage devices are separate units, which reduce the power density and limit their applications. Therefore, researchers are aiming to propose

^aNational Key Lab of Nano/Micro Fabrication Technology, Peking University, Beijing, 100871, China. E-mail: zhang-alice@pku.edu.cn

^bAcademy for Advanced Interdisciplinary Studies, Peking University, Beijing, 100871, China

† Electronic supplementary information (ESI) available. See DOI: 10.1039/c6ta05816g

a new hybrid system that integrates an energy-harvesting device along with a storage device to perform a self-powered operation.^{34,35} Recently, Wang *et al.* developed a multi-TEG stacked self-charging system,³⁶ in which the mechanical energy can be directly converted into electrochemical energy; however, the improvement in performance is at the expense of the volume increasing. Meanwhile, for relatively low space utilization, the integration of such a self-charging unit still has plenty of room for enhancement.

Herein, we demonstrate a hybrid sandwich-shaped, self-charging power unit (SCPU) involving both the energy-harvesting and storage devices. Considering the fact that an optimized single-step fluorocarbon plasma process on polydimethylsiloxane (PDMS) can form wrinkle structures with high triboelectric output ability³⁷ and carbon nanotubes (CNTs) own excellent electrochemical properties as SC electrodes,³⁸ our device integrates wrinkled PDMS-based TENG and CNT-based solid-state SC. The high degree of integration is realized through the TENG-SC-TEG design, which could take advantage of both the top and bottom surfaces of SC and greatly decrease the unit's volume. When compressive stress is applied to the SCPU, the mechanical energy is directly converted into electrical energy and stored in the SC efficiently. Once fully charged, three serial SCPUs can continuously power an electrochromic device as a smart window or a commercial calculator. Therefore, this SCPU shows promising potential in flexible displays, wearable devices and various sensor systems.

Experimental

Fabrication of wrinkled PDMS-based TENG

The elastomer and cross-linker of commercial PDMS (Sylgard 184, Dow Corning Co.) were mixed with a quantity ratio of 5 : 1. The vacuum-degassed PDMS mixture was spin-coated on an indium tin oxide (ITO)/polyethylene terephthalate (PET) film (4 cm × 5 cm). Then, fluorocarbon (C₄F₈) plasma treatment of the uncured PDMS surface was conducted using an inductively coupled plasma (ICP) etcher, forming a wrinkled structure in the process. The RF power, plate power, gas flow rate, pressure and treatment time were optimized to 0 W, 100 W, 60 sccm, 5 Pa and 150 s, respectively. After the PDMS was cured at 90 °C for 30 min as a triboelectric layer, the arch-shaped TENG was then assembled with processed PDMS/ITO/PET film and another ITO/PET film, in which the PET layer was bent to enhance the output and the ITO layer was used as both the triboelectric layer and electrode. The gap size of the fabricated TENG was fixed at 3 mm, and when both layers were fully contacted, the size of each TENG was 40 mm × 50 mm × 0.3 mm, saving more than 50% volume compared with other TENGs³⁶ and greatly improving the integration degree.

Fabrication of flexible solid-state SC

The flexible CNT/paper electrodes were fabricated simply by using the drop-drying method. Firstly, CNT ink solution was prepared by dispersing CNTs (20 mg, Boyu Co., China) and 20 mg sodium dodecylbenzenesulfonate (SDBS) as surfactant in

20 ml of deionized water. After the CNT ink solution was bath-sonicated for 4 h to disperse evenly, approximately 10 ml of the CNT ink was dropped on a filter paper with an area of 2 cm × 2 cm and dried at 80 °C for 1 h in an oven. This drop-drying process was repeated several times. The average mass of the filter paper was about 32 mg in the initial state. Then, after several CNT ink drop-dry processes, the average mass of the CNT/paper electrode increased to 48 mg, which showed that approximately 8 mg CNTs were dropped on a filter paper as the active materials, leading to a CNT density of 2 mg cm⁻². Additionally, 6 g phosphoric acid (H₃PO₄) was mixed with 60 ml deionized water and 6 g polyvinyl alcohol (PVA) powder. The mixture was heated up to 85 °C under vigorous stirring until the solution became clear. After the solution cooled down, two pieces of flexible CNT/paper electrodes were coated with PVA/H₃PO₄ gel electrolyte, and then assembled into a symmetrical SC with a cellulose separator (TF44, NKK Co., Japan). The flexible solid-state device was subsequently left in the fume hood at room temperature to fully vaporize the excess water.

Fabrication of self-charging power unit

To eliminate the electrostatic induction and signal interference between the TENG and SC, SC was packaged with PDMS mixture (elastomer and cross-linker with a ratio of 10 : 1) as insulator film and cured at 80 °C for 1 h with an area of 4 cm × 5 cm. Additionally, both the top and bottom surfaces of the packaged device were adhered to the ITO/PET film of the arch-shaped TENG to assemble the sandwich-shaped SCPU. When fully compressed, the dimensions of the entire device were only 4 mm × 5 cm × 4 mm, respectively. Additionally, two TENGs were connected in parallel to enhance the triboelectric output and charging efficiency.

Characterization

The structure and morphology of the materials were characterized using scanning electron microscopy (SEM), and laser scanning microscope (LSM) was also employed to characterize the PDMS structure change under C₄F₈ plasma treatment. Additionally, the output voltage of the TENG was measured *via* a digital oscilloscope (Agilent DSO-X 2014A) using a 100 MΩ probe (HP9258), and the current was amplified by a SR570 low-noise current amplifier from Stanford Research Systems. For the electrochemical measurement of the SC, an electrochemical workstation (CHI660) was utilized by using CV and GCD techniques with a two-electrode configuration. To characterize the self-charging properties of the power unit, a sinusoidal signal was generated from the signal source module of the digital oscilloscope and amplified by an amplifier (SINOCERA YE5871A) to power the modal shaker (JZK-10), which could apply a cycled and stable compressive force to the SCPU with a fixed frequency of 8 Hz.

Results and discussion

As illustrated in Fig. 1, this self-charging power unit is fabricated by integrating a wrinkled PDMS-based TENG and CNT/

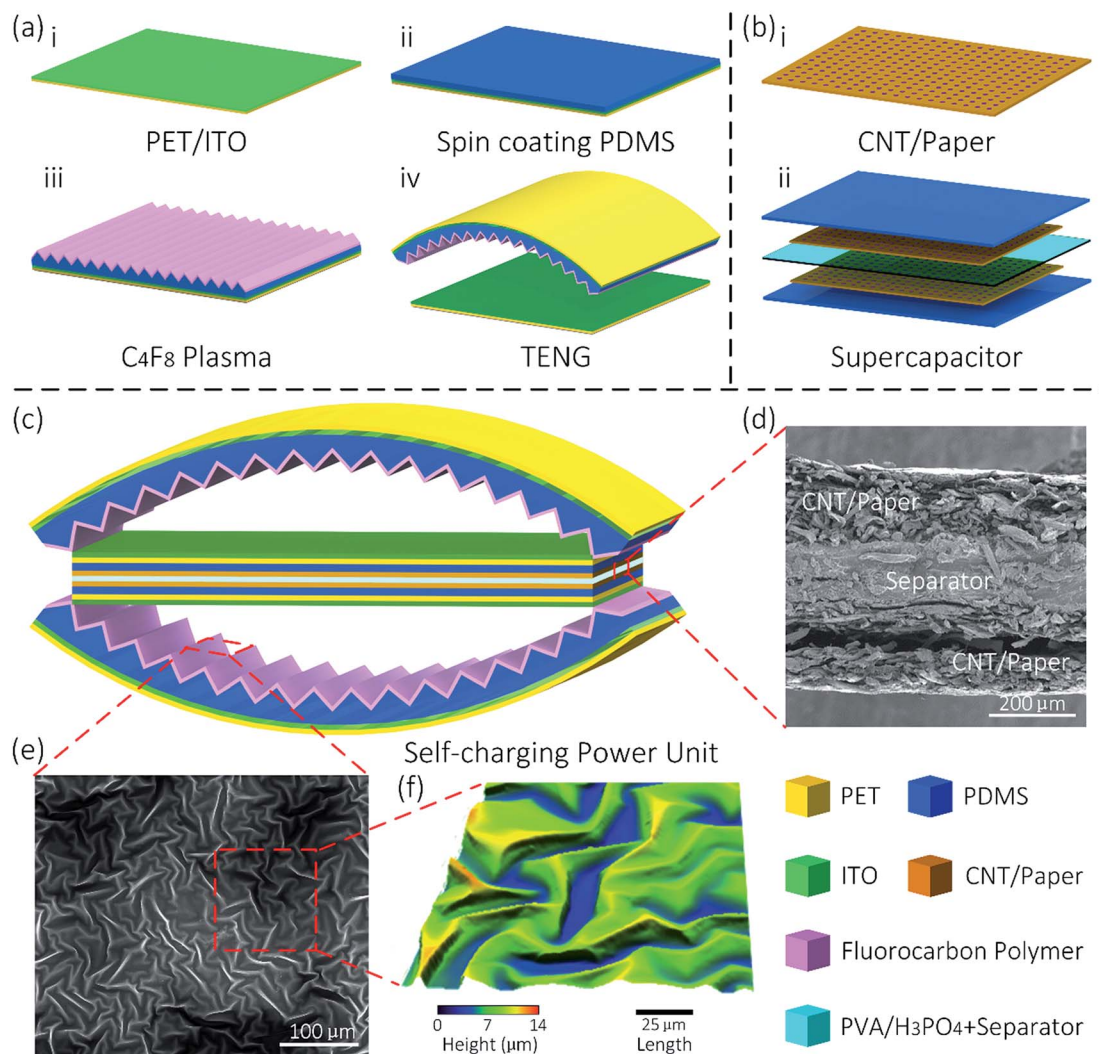


Fig. 1 (a) Schematic diagram of the fabrication process of arch-shaped TENG, which includes spin-coating PDMS on PET/ITO film, C_4F_8 plasma treatment to form the wrinkled structure, and its assembly process. (b) The fabrication process of PDMS packaged solid-state SC, which is composed of CNT/paper electrode, gel electrolyte and separator. (c) The structure design of sandwich-shaped SCPU. (d) The SEM image of the cross-section of the solid-state SC. (e) The SEM image of the wrinkled structure and (f) the LSM image of its 3D morphology.

paper-based, solid-state SC. In detail, Fig. 1a shows the fabrication process of the TENG. It starts with an ITO-coated PET film, which works as both the flexible substrate and electrode, where the vacuum-degassed PDMS mixture is then spin-coated on it. Before the PDMS mixture is cured, a C_4F_8 plasma treatment process is carried out in an ICP etching machine, during which time the wrinkle structure is formed. The detailed fabrication of this wrinkle structure is also discussed in Fig. S1 (ESI[†]), which results in efficiently increased triboelectric charge density through surface modification and microstructure effect. To compose an arch-shaped TENG, the processed cured PDMS film is then assembled with another PET/ITO film.

In solid-state SC, CNT ink is drop-dried on the paper several times as the active material and electrode, while TF44 film and H_3PO_4 /PVA gel are adopted as separator and electrolyte (Fig. 1b). After those components are assembled into a solid-state SC, the processed device is fully packaged with PDMS

mixture. As for CNT percolation during the drop-dry process, relative simulation results are shown in Fig. S2 (ESI[†]). The typical morphology of the CNT/paper is characterized by SEM as showing relatively uniform coating in Fig. S3 (ESI[†]). The detailed device structure of the SCPU is schematically depicted in Fig. 1c, which is composed of two arch-shaped TENGs and a packaged solid-state SC. Fig. 1d demonstrates the cross-sectional SEM image of the sandwiched structure of the SC. The processed wrinkled structure is characterized by SEM, and its 3D view is attained by LSM, shown in Fig. 1e and f, respectively.

Output characterization of TENG

The performance of the single wrinkled PDMS-based, arch-shaped TENG under periodic impacts with different frequencies is investigated *via* a vibration system. The TENG works well over a frequency range of 2 Hz to 10 Hz. Continuous periodic outputs are generated, which prove quite uniform and fairly

symmetrical. Obviously, the frequency of the output wave matches the frequency of excitation. The open-circuit voltage (V_{OC}) and short-circuit current (I_{SC}) waveforms at different frequencies are illustrated in Fig. 2a and b separately. As the frequency increases, both V_{OC} and I_{SC} become larger, which accounts for the fact that external electrons flowing reached equilibrium more quickly. Specially, under the frequency of 10 Hz, the single arch-shaped TENG's V_{OC} attains more than 200 V, with I_{SC} around 100 μA . In addition, the device obtains good stability for 30 000 cycles as shown in Fig. S4 (ESI†), maintaining almost the same output and satisfying the needs of a stable charging process. The charging ability of TENG is evaluated by charging a 1 μF capacitor through a full-wave rectifier bridge to nearly 0.6 V in a single operation cycle (Fig. 2c).

Considering the fact that simply stacked TENG structures will inevitably increase the device's volume and limit unit integration, a novel TENG-SC-TENG sandwich-shaped structure is designed to simultaneously take advantage of the top and bottom surfaces of the SC. The two wrinkled PDMS-based TENGs are connected in parallel to simultaneously improve the output voltage and current. Compared to the single TENG, the performance of the paralleled TENGs is also investigated under the same conditions. As shown in Fig. 2d, when the external stress frequency increases from 2 Hz to 5 Hz, the V_{OC} also increases from 300 to 320 V because it takes a shorter time to reach external electron equilibrium. Then, the V_{OC} continuously decreases to 230 V under 10 Hz external stress frequency due to the under-release of the sandwich-shaped TENGs. If the compressive stress cycle is too short (*i.e.*, frequency is too high),

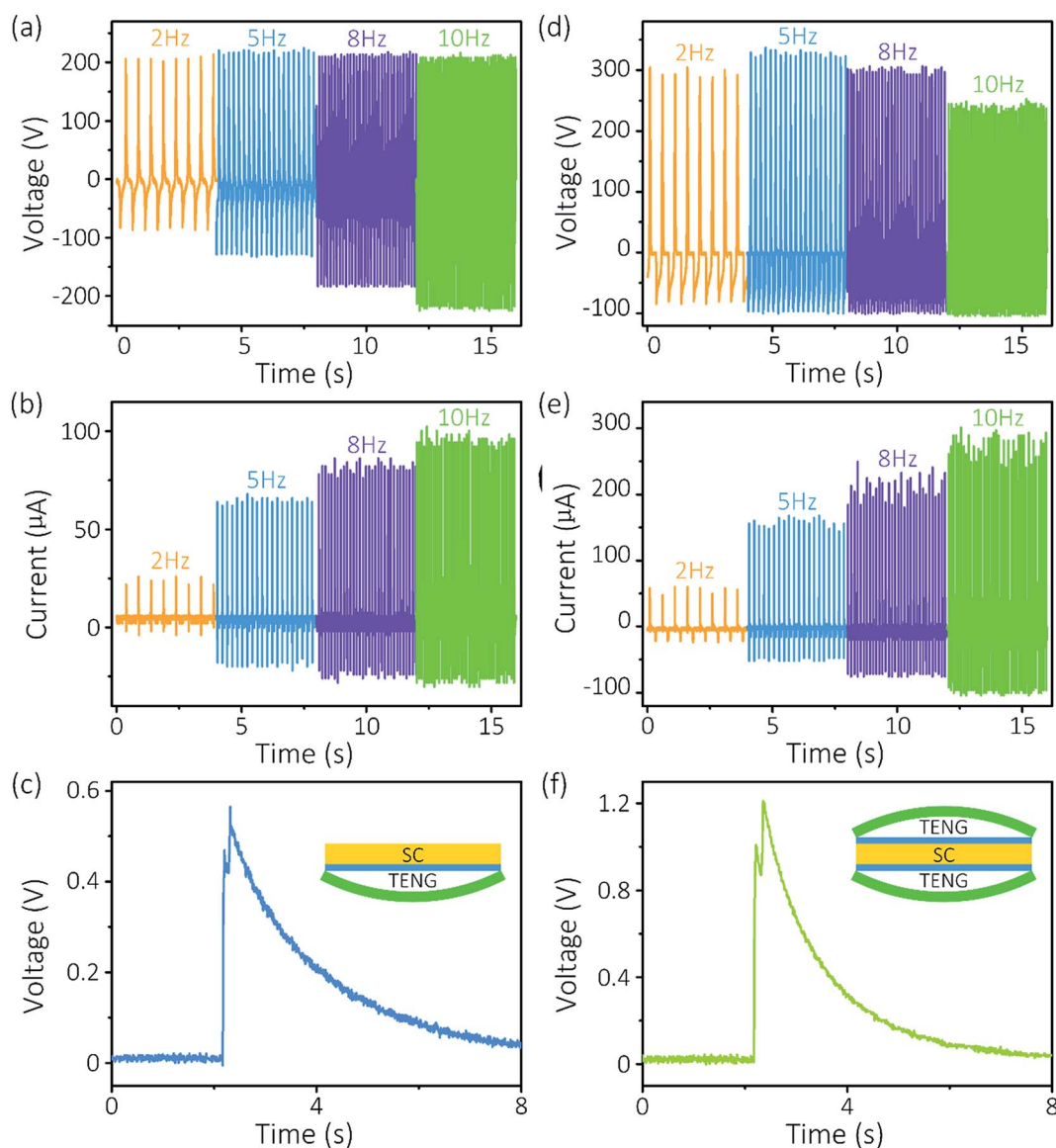


Fig. 2 Output characterization of the TENG. (a) The output voltage and (b) current waveforms of a single arch-shaped TENG at various frequencies. (c) The charging curve of a 1 μF capacitor of a single TENG. (d) Output voltage and (e) current waveforms of 2-parallel connection TENGs at various frequencies. (f) The charging curve of a 1 μF capacitor of 2-parallel connection TENGs.

the TENGs cannot recover to the original position before the next impact. Generally speaking, TENGs connected in parallel could increase V_{OC} to some degree. As for the correlation between I_{SC} and frequency, Fig. 2e shows that I_{SC} is consistent with the changing frequency. It is worth noting that under frequency of 10 Hz, the parallel-connection TENGs' I_{SC} reaches nearly 300 μA , which is an obvious enhancement in contrast to the single TENG. This enhancement can also be proven by charging the same 1 μF capacitor to 1.2 V through a full-wave rectifier in a single operation cycle (Fig. 2f). The total amount of transferred charges also more than doubles that of the single arch-shaped TENG. It accounts for the fact that parallel-connection TENGs could coordinate with each other and jointly improve output performance. Therefore, such sandwich-shaped design is beneficial to raising the integration degree and efficiently harvesting energy from ambient vibrations.

Electrochemical behaviour of SC

To further evaluate the electrochemical performance, the CNT/paper-based, flexible solid-state SC is carefully characterized through cyclic voltammetry (CV) and galvanostatic charge-discharge (GCD) measurements *via* electrochemical workstation. As mentioned before, the SC is packaged with PDMS to eliminate the interference of the TENG signal. The fabricated device is compact, and more importantly, it exhibits excellent flexibility and stability both in mechanical properties and electrochemical performance, as shown in Fig. 3. Firstly, electrochemical performance of the SC device is analyzed by CV

curves at a stable potential window between 0 and 1 V (Fig. 3a). Under the scan rates from 10 mV s^{-1} to 200 mV s^{-1} , the CV curves retain quasi-rectangular shape and are approximately symmetrical about the zero-current line, indicating fast charging-discharging rate and an ideal electrochemical behaviour. Then, GCD curves are also measured at various current densities shown in Fig. 3b, the charging-discharging current densities of which are from 0.1 mA cm^{-2} to 4 mA cm^{-2} . Discharge profile of the fabricated supercapacitor is dependent on the applied current, and similar curve shapes have been obtained for different current densities. Both the linear profile of the charging-discharging curves and their symmetry reveal the superior electrochemical characteristics of the solid-state SC device. This fast charging ability enables it to respond to the pulse output of TENG swiftly and stably supply the low-power device.

Besides, the areal capacitance (C_A) is calculated by the following equations according to the CV curves of SC:

$$C = \frac{Q}{\Delta V} = \frac{1}{k\Delta V} \int_{V_1}^{V_2} I(V)dV \quad (1)$$

$$C_A = \frac{C}{A} = \frac{1}{kA\Delta V} \int_{V_1}^{V_2} I(V)dV, \quad (2)$$

where C is the total capacitance, $I(V)$ is the charge-discharge current function, k is the scan rate, A is the area of the SC and ΔV is the potential window during the discharge process, where V_1 and V_2 are maximum and minimum voltage values, respectively.

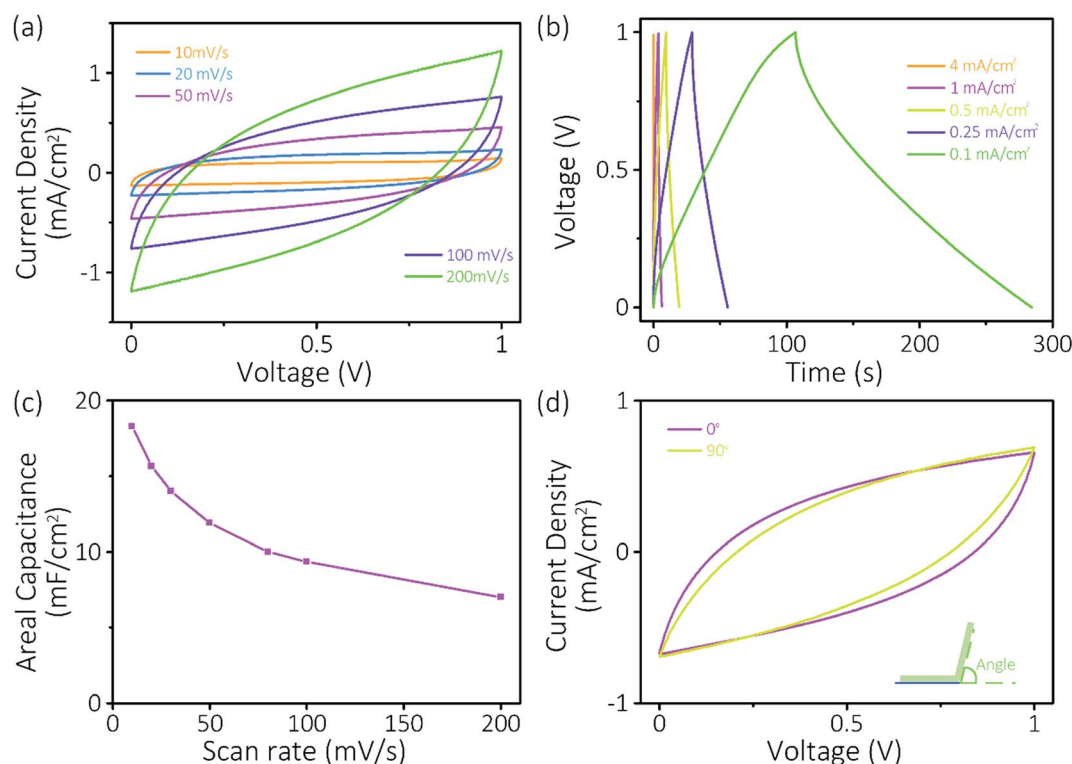


Fig. 3 Electrochemical behaviour of the SC. (a) CV curves at different scan rates and (b) GCD curves at different current densities of the device. (c) Calculated areal capacitance as a function of voltage scan rate. (d) CV curves of device at different conditions (flat and bent).

The maximum areal capacitance is 18.3 mF cm^{-2} at scan rate of 10 mV s^{-1} , and this solid-state SC could withstand the charging–discharging process without significant degradation in areal capacitance even at high scan rate (Fig. 3c), thus demonstrating a stable electrochemical performance. Additionally, to prove the feasibility of the solid-state SC as a flexible energy storage device and for self-powered systems, electrochemical performance is further tested under bending angles. Undoubtedly, with the strong protection of the PDMS package layer, neither the configuration nor the CV curves (Fig. 3d) of the SC device experience obvious changes under different test conditions, confirming that the device has outstanding mechanical flexibility. Meanwhile, the SC also shows excellent stability under CV test at a scan rate of 100 mV s^{-1} for 4000 cycles, and the result is shown in Fig. S5 in the ESI.† It indicates that the capacitance of the device increases at the beginning of the test due to the electrode self-activation process, and then degenerates gradually and remains at about 134% after 4000 cycles compared with the first cycle. Therefore, the packaged SC demonstrates stable and excellent electrochemical performance and satisfies the needs of a self-charging power unit.

Working mechanism of SCPU

Fig. 4 demonstrates the working mechanism of this sandwich-shaped SCPU under vertical contact-separation mode. At the original state, no electrical potential exists between the

triboelectric pairs, ITO layer and PDMS layer, as shown in Fig. 4a. Due to the specially designed sandwich-shaped structure, once a periodic compressive stress is applied, ITO and PDMS will contact twice and transfer electrons between them, thus doubling the frequency of the output. In detail, when the SCPU is stressed, the top wrinkled PDMS layer first contacts the ITO layer; ITO loses electrons while PDMS gets negative charges, according to the triboelectric series. With proper external rectifier connections, the potential difference between ITO and PDMS drives the electron flow to charge the sandwiched SC (Fig. 4b). Soon afterward, the bottom wrinkled PDMS layer contacts the ITO layer, generating a current flow in the same direction (Fig. 4c) until the device reaches electrical equilibrium.

When the stress is released, SCPU tends to recover to the original state, and the distributed charges build a reversed potential as the gap distance increases. Once the ITO layer leaves the bottom PDMS layer, positive charges are induced on the back ITO electrode, thus driving electrons to flow through the external circuit in the opposite direction and producing the first peak output (Fig. 4d). Subsequently, the separation of the top PDMS and ITO layers brings the second peak output (Fig. 4e), and the device reaches equilibrium again, thus completing a self-charging cycle. Specially, the output voltage from the TENG is rectified by a rectifier bridge, transforming the alternating current (AC) to direct current (DC), thus

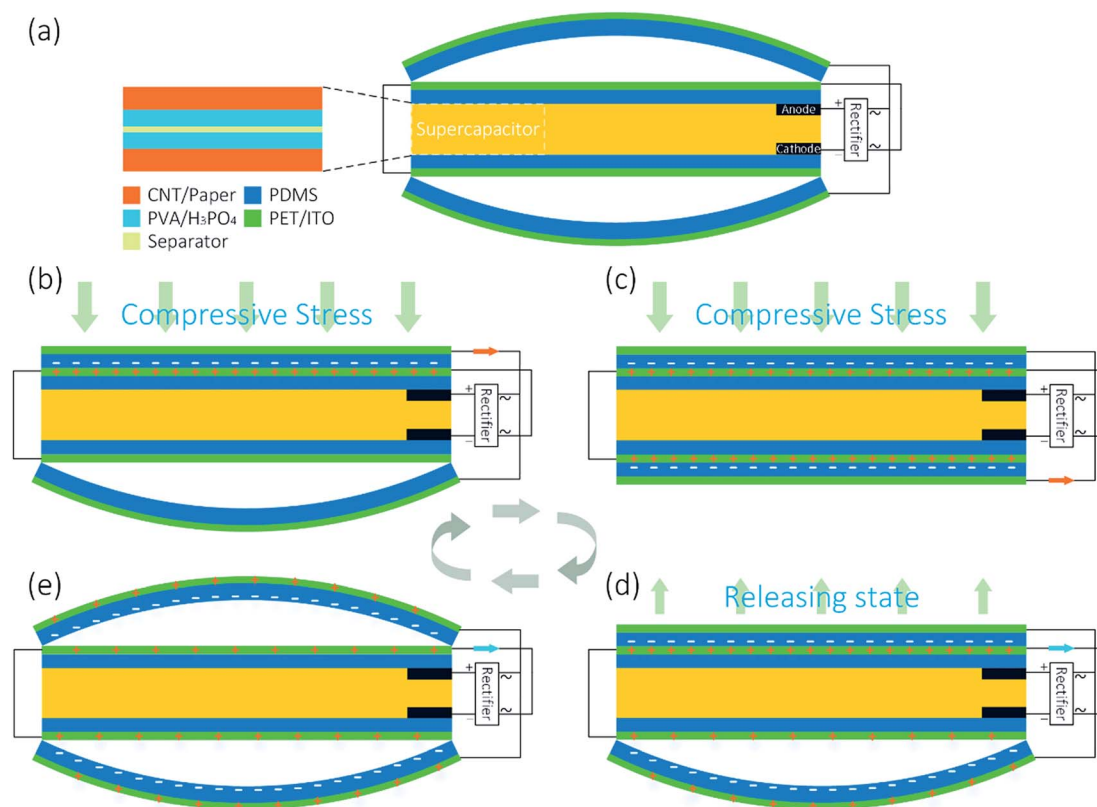


Fig. 4 Schematic diagram showing the electrical distribution and working mechanism of the sandwich-shaped SCPU from (a) the original state, (b) stressed state, (c) completed stressed state, to (d) the releasing state and (e) back to original state.

continually charging the SC. Under a 2 Hz compressive stress, two upward and downward peaks with unequal amplitudes can be clearly observed in the output voltage signal, as shown in Fig. S6 (ESI[†]). It is worth mentioning that the downward peaks may be overlapped due to the rapidly applied stress.

Self-charging performance of SCPU

As for the TENG–SC–TENG self-charging power unit, TENGs connected in parallel are utilized to charge the SC *via* a rectifier and a switch S1, and then an external load is connected through the other switch S2 (Fig. 5a). While working in the energy-harvesting mode (S1 on and S2 off), the TENG, triggered by a shaker, can convert the mechanical energy to electrical energy and store it in the SC component. As shown in Fig. 5b, the charging rate of SCPU increases with the compressive stress frequency. When the SC is charged by two parallel connected TENGs, it can be directly charged to 120 mV within 250 s under 10 Hz, which demonstrates excellent charging efficiency. Compared with the initial charging curves of the single TENG, which is displayed in Fig. S7 (ESI[†]), such TENG–SC–TENG design could significantly increase the charging rate. Then, under the periodic compressive stress of 8 Hz, the entire charging fitting curve of the SC is shown in Fig. 5c, where the stored charges steadily increase with the charging time, and the potential eventually reaches 900 mV in 3 h.

Besides, when a sufficient amount of charge has been stored during the energy storage mode, the SCPU will transform to the

energy supply mode (S1 off and S2 on). Three as-fabricated SCPUs (optical image shown in Fig. 6a) are connected in series, and when fully charged, the three SCs could drive a calculator to perform a series of calculations. The calculator could stably work the complex arithmetic for more than 40 minutes (Fig. S8 in the ESI[†]), which demonstrates that the SCPU can sustainably drive a low-powered electric device. Additionally, the SCPU could also supply an electrochromic device (ECD) as a self-

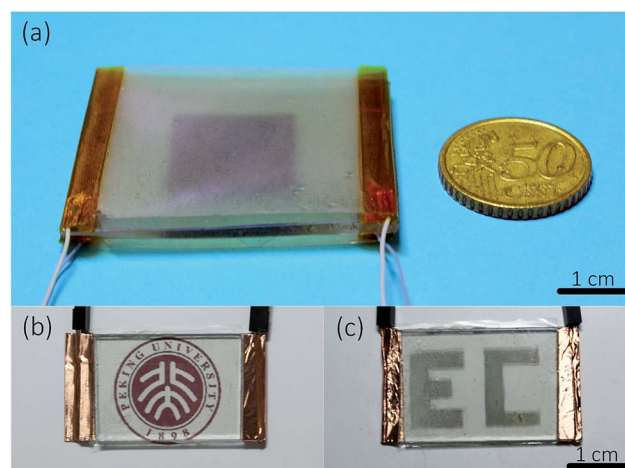


Fig. 6 (a) Optical image of the SCPU. An ECD driven by SCPU with (b) bleaching and (c) coloration process as a smart window.

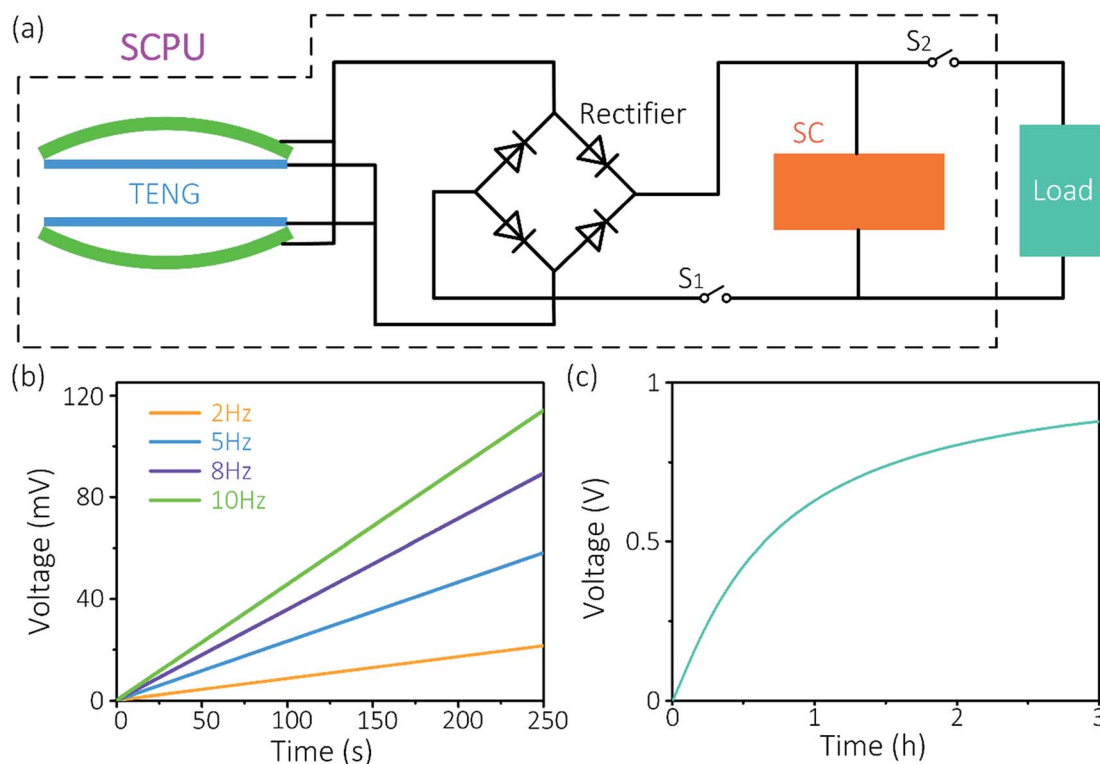


Fig. 5 Self-charging performance of SCPU. (a) Circuit diagram of the SCPU with energy storage and supply mode. (b) Initial charging curves of the sandwiched SC charged by sandwich-shaped, parallel-connected TENGs at various frequencies. (c) Charging curve of the SC charged by sandwich-shaped TENGs at the compressive stress of 8 Hz.

powered smart window (detailed schematic diagram and fabrication of ECD are provided in Fig. S9 in the ESI†). In this system, the coloration and bleaching loops are controlled by the S2 switch. When the S2 switch closes to a coloration process and SCs connect the ITO electrodes of ECD, the smart window changes its colour from colourless to black due to the fact that the dissolved Ag^+ ion deposits on the ITO electrode undergoing a redox process, showing the designed pattern clearly (Fig. 6c). Conversely, the ECD smart window reverts to transparency with the bleaching process, where the Ag begins to dissolve in the electrolyte when the S2 switch is off (Fig. 6b). As a result, the SCPU-charged ECD self-powered smart window could reversibly change its colour during the charge–discharge process, which can be potentially applied in buildings, cars and displays.

Conclusions

In summary, we propose a self-charging power unit that integrates wrinkled PDMS-based TENG as energy-harvesting device and solid-state SC as energy storage device. The TENG–SC–TENG sandwich-shaped structure could definitely improve the integration because this design can take advantage of both the top and bottom surfaces of SC and greatly decrease the unit's volume. On one hand, with the wrinkled PDMS structure enlarging the contact area efficiently and the parallel device connection, the output performance of TENG is greatly boosted, achieving a short-circuit current of nearly 300 μA . On the other hand, the solid-state SC shows excellent stability and mechanical strength, which enables it as a promising flexible energy storage device. During ambient vibrations, the SCPU can be utilized to simultaneously harvest and store the mechanical energy into electrochemical energy, charged to 900 mV in 3 h under the compressive stress of 8 Hz. When fully charged, three integrated SCPU in series connection could continuously power a calculator. Besides, with a control switch, an electrochromic device can be driven as a smart window during the coloration and bleaching process, which has potential applications in smart homes and various displays. Therefore, with high integration and excellent performance, this novel SCPU is a promising candidate in flexible electronics and wearable devices and definitely exerts a significant impact in self-powered systems research.

Acknowledgements

This work is supported by the National Natural Science Foundation of China (Grant No. 61674004, 61176103 and 91323304), National Key R&D Project from Minister of Science and Technology, China (2016YFA0202701), the Beijing Science & Technology Project (Grant No. Z141100003814003) and the Beijing Natural Science Foundation of China (Grant No. 4141002).

References

- M. S. Dresselhaus and I. L. Thomas, *Nature*, 2001, **414**, 332–337.
- S. M. Yang, T. Lee and C. A. Jeng, *Sens. Actuators, A*, 2009, **153**, 244–250.
- M. E. Himmel, S. Y. Ding, D. K. Johnson, W. S. Adney, M. R. Nimlos, J. W. Brady and T. D. Foust, *Science*, 2007, **315**, 804–807.
- N. S. Lewis, *Science*, 2007, **315**, 798–801.
- S. P. Beeby, M. J. Tudor and N. M. White, *Meas. Sci. Technol.*, 2006, **17**, R175–R195.
- M. Ha, J. Park, Y. Lee and H. Ko, *ACS Nano*, 2015, **9**, 3421–3427.
- T. Quan, X. Wang, Z. L. Wang and Y. Yang, *ACS Nano*, 2015, **9**, 12301–12310.
- Y. Zi, L. Lin, J. Wang, S. Wang, J. Chen, X. Fan, P. K. Yang, F. Yi and Z. L. Wang, *Adv. Mater.*, 2015, **27**, 2340–2347.
- M. Tsang, A. Armutlulu, A. W. Martinez, S. A. B. Allen and M. G. Allen, *Microsystems & Nanoengineering*, 2015, **1**, DOI: 10.1038/micronano.2015.24.
- X. Wang, J. Song, J. Liu and Z. L. Wang, *Science*, 2007, **316**, 102–105.
- S. M. Cha, J. S. Seo, S. M. Kim, H. J. Kim, Y. J. Park, S. W. Kim and J. M. Kim, *Adv. Mater.*, 2010, **22**, 4726–4730.
- P. Glynne-Jones, M. J. Tudor, S. P. Beeby and N. M. White, *Sens. Actuators, A*, 2004, **110**, 344–349.
- J. D. Chen, D. Chen, T. Yuan and X. Chen, *Appl. Phys. Lett.*, 2012, **100**, 213509.
- L. G. W. Tvedt, D. S. Nguyen and E. Halvorsen, *J. Microelectromech. Syst.*, 2010, **19**, 305–316.
- P. Basset, D. Galayko, A. M. Paracha, F. Marty, A. Dudka and T. Bourouina, *J. Micromech. Microeng.*, 2009, **19**, 115025.
- F. R. Fan, Z. Q. Tian and Z. L. Wang, *Nano Energy*, 2012, **1**, 328–334.
- X. S. Zhang, M. D. Han, R. X. Wang, F. Y. Zhu, Z. H. Li, W. Wang and H. X. Zhang, *Nano Lett.*, 2013, **13**, 1168–1172.
- B. Meng, W. Tang, Z. H. Too, X. Zhang, M. Han, W. Liu and H. Zhang, *Energy Environ. Sci.*, 2013, **6**, 3235–3240.
- G. Qiu, W. Liu, M. Han, X. Cheng, B. Meng, A. Smitha, J. Zhao and H. Zhang, *Sci. China: Technol. Sci.*, 2015, **58**, 842–847.
- M. Han, B. Yu, G. Qiu, H. Chen, Z. Su, M. Shi, B. Meng, X. Cheng and H. Zhang, *J. Mater. Chem. A*, 2015, **3**, 7382–7388.
- M. D. Han, X. S. Zhang, B. Meng, W. Liu, W. Tang, X. M. Sun, W. Wang and H. X. Zhang, *ACS Nano*, 2013, **7**, 8554–8560.
- M. D. Huntington, C. J. Engel, A. J. Hryn and T. W. Odom, *ACS Appl. Mater. Interfaces*, 2013, **5**, 6438–6442.
- M. D. Huntington, C. J. Engel and T. W. Odom, *Angew. Chem.*, 2014, **126**, 8255–8259.
- P. Simon and Y. Gogotsi, *Nat. Mater.*, 2008, **7**, 845–854.
- J. R. Miller and P. Simon, *Science*, 2008, **321**, 651–652.
- X. Lu, M. Yu, T. Zhai, G. Wang, S. Xie, T. Liu, C. Liang, Y. Tong and Y. Li, *Nano Lett.*, 2013, **13**, 2628–2633.
- X. Lu, M. Yu, G. Wang, Y. Tong and Y. Li, *Energy Environ. Sci.*, 2014, **7**, 2160–2181.
- Y. J. Kang, H. Chung, C. H. Han and W. Kim, *Nanotechnology*, 2012, **23**, 065401.
- S. He, H. Hou and W. Chen, *J. Power Sources*, 2015, **280**, 678–686.

- 30 Y. Chen, X. Zhang, D. Zhang, P. Yu and Y. Ma, *Carbon*, 2011, **49**, 573–580.
- 31 X. Xiao, T. Li, P. Yang, Y. Gao, H. Jin, W. Ni, W. Zhan, X. Zhang, Y. Cao, J. Zhong, L. Gong, W. C. Yen, W. Mai, J. Chen, K. Huo, Y. L. Chueh, Z. L. Wang and J. Zhou, *ACS Nano*, 2012, **6**, 9200–9206.
- 32 S. Niu, X. Wang, F. Yi, Y. S. Zhou and Z. L. Wang, *Nat. Commun.*, 2015, **6**, 8975–8982.
- 33 B. Shi, Q. Zheng, W. Jiang, L. Yan, X. Wang, H. Liu, Y. Yao, Z. Li and Z. L. Wang, *Adv. Mater.*, 2015, **28**, 846–852.
- 34 J. Luo, F. R. Fan, T. Jiang, Z. W. Wang, W. Tang, C. P. Zhang, M. M. Liu, G. Z. Cao and Z. L. Wang, *Nano Res.*, 2015, **8**, 3934–3943.
- 35 R. Song, H. Jin, X. Li, L. Fei, Y. Zhao, H. Huang, H. Chan, Y. Wang and Y. Chai, *J. Mater. Chem. A*, 2015, **3**, 14963–14970.
- 36 J. Wang, Z. Wen, Y. Zi, P. Zhou, J. Lin, H. Guo, Y. Xu and Z. L. Wang, *Adv. Funct. Mater.*, 2016, **26**, 1070–1076.
- 37 X. Cheng, B. Meng, X. Chen, M. Han, H. Chen, Z. Su, M. Shi and H. Zhang, *Small*, 2016, **12**, 229–236.
- 38 Y. Song, X. Cheng, H. Chen, M. Han, X. Chen, J. Huang, Z. Su and H. Zhang, *Micro Nano Lett.*, 2016, DOI: 10.1049/mnl.2016.0255.